Original Paper

Indoor and Built Environment

Indoor and Built Environment
0(0) 1–14

DOI: 10.1177/1420326X16631596
ibe.sagepub.com

SAGE

Ventilation of general hospital wards for mitigating infection risks of three kinds of viruses including Middle East respiratory syndrome coronavirus

H.C. Yu, K.W. Mui, L.T. Wong and H.S. Chu

Abstract

This study investigates the effectiveness of ventilation design strategies for general hospital wards in terms of virus removal capacity. A typical semi-enclosed six-bed general ward of Hong Kong hospitals and three respiratory viruses, namely Middle East respiratory syndrome coronavirus (MERS-*CoV*), severe acute respiratory syndrome coronavirus (SARS-*CoV*) and H1N1 influenza virus, were chosen for the computational fluid dynamics (CFD) simulation of airflow field and virus dispersion inside the ward. The results demonstrated that the location of an infected patient would affect the infection risks to other occupants and healthcare workers inside the same hospital ward, and an increased air change rate in the ward could reduce the risk of infection from direct contact and inhalation. It was found that an air change rate of $9\,h^{-1}$ could effectively minimize the deposition and floating time of respiratory virus particles while maximizing energy efficiency. This study should provide a useful source of reference for the hospital management to mitigate the risk of infection with MERS or other airborne transmitted viruses through better ventilation design strategies.

Keywords

Ventilation, Virus dispersion, Hospital general wards, CFD, Middle East respiratory syndrome (MERS)

Accepted: 4 January 2016

Introduction

According to a statistical report by the Hong Kong Hospital Authority,[1] the in-patient discharges and deaths were continuously increasing from 2003 to 2013. The 2012/2013 overall number of in-patient discharges and deaths was 1,027,005, and that of day-patient was 516,127 in Hong Kong. Among all patients, 33.4% were day-patients.

To prevent nosocomial or healthcare-associated infections, especially airborne ones, hospital hygiene and infection control are necessary. The Centres for Disease Control and Prevention (CDC) provides guidance to help healthcare personnel to follow standard, contact, and airborne precautions when caring for hospitalized patients with known or suspected viral infections.[2] Effective prevention measures, e.g. an airborne infection isolation room (AIIR), are especially crucial for control of acute respiratory infectious threats.

Proper ventilation also plays a key role in infection control by minimizing airborne bacteria and viruses. Both the spread of severe acute respiratory syndrome coronavirus (SARS-*CoV*) during the largest nosocomial SARS outbreak in Hong Kong and the recent outbreak of Middle East respiratory syndrome (MERS) in the South Korean hospitals revealed that airborne disease transmission through inefficient hospital ward ventilation systems can lead to dire health consequences.[3–5] For a balanced ventilation that delivers indoor air

Department of Building Services Engineering, The Hong Kong Polytechnic University, Hong Kong, China

Corresponding author:
L. T. Wong, Department of Building Services Engineering, The Hong Kong Polytechnic University, Hong Kong, China.
Email: beltw@polyu.edu.hk

quality and energy efficiency, general hospital wards have been designed to meet certain air change requirements.[2,6–10] For instance, an air change rate (*ach*) ranging from 2 to 6 h^{-1} is suggested to help decrease local mean age of air,[11] while 4 h^{-1} is recommended for energy savings.[12,13] However, as new information becomes available, current air change requirements for hospital wards should be re-evaluated and updated.

This study investigates the effectiveness of ventilation design strategies for general hospital wards in terms of virus removal capacity. A computational fluid dynamics (CFD) simulation of a typical general ward of Hong Kong hospitals was conducted and three respiratory viruses, namely MERS-*CoV*, SARS-*CoV* and H1N1 influenza virus, were chosen. The findings can be used by the hospital management to minimize cross-infection risk while reducing energy consumption of ventilation.

Bioaerosol drag force

The motions of spherical and non-spherical bioaerosols in a ventilated space can be calculated using equation (1) by integrating the force balance on the bioaerosols in terms of the drag force per unit particle mass per relative velocity F_D (N s kg^{-1} m^{-1}), where g is gravitational acceleration (m s^{-2}), F_x is the additional acceleration force per unit particle mass (N kg^{-1}) if any, v_b and v_a are the velocities of the virus and air (m s^{-1}), respectively, μ_a is the molecular viscosity of air (kg m^{-1} s^{-1}), d_b is the equivalent bioaerosol diameter (μm), Re_b is the Reynolds number for bioaerosols in an airflow field, ρ_a is the air density (kg m^{-3}) and ρ_b is the virus density (=1100 kg m^{-3}).[14]

$$\frac{dv_b}{d\tau} = F_D(v_a - v_b) + \frac{g(\rho_b - \rho_a)}{\rho_b} + F_x; \quad F_D = \frac{18\mu_a}{d_b^2\rho_b} \times \frac{C_D Re_b}{24};\ Re_b = \frac{\rho_a d_b |v_b - v_a|}{\mu_a} \tag{1}$$

The drag coefficient C_D for the bioaerosols is defined by equation (2)

$$C_D = \frac{K_D}{Re_b};\ Re_b < 1 \tag{2}$$

Equations (1) and (2) are used in the CFD simulation to determine the motions of droplet nuclei under a Lagrangian scheme.

The drag constant for the bioaerosols K_D in equation (2) is given by equation (3)

$$K_D = \frac{d_b^2}{2} \tag{3}$$

Validity of equation (3) was established for equivalent bioaerosol diameters $d_b = 0.69$–$6.9\,\mu$m over a bioaerosol size range and further examined for *Bacteriophage Phi X174* (ATCC 13706-B1) with $d_b = 0.054\,\mu$m. A combined experimental and simulation method described by Wong et al.[14] was performed. Before the experiment, agar plates were prepared in such a way that the entire preparation was covered by the host bacterium *Escherichia coli* (ATCC 13706). Plaque assays for bacteriophages were then conducted. The number of bacteriophages collected was measured by plate counting.[15] Figure 1 shows that

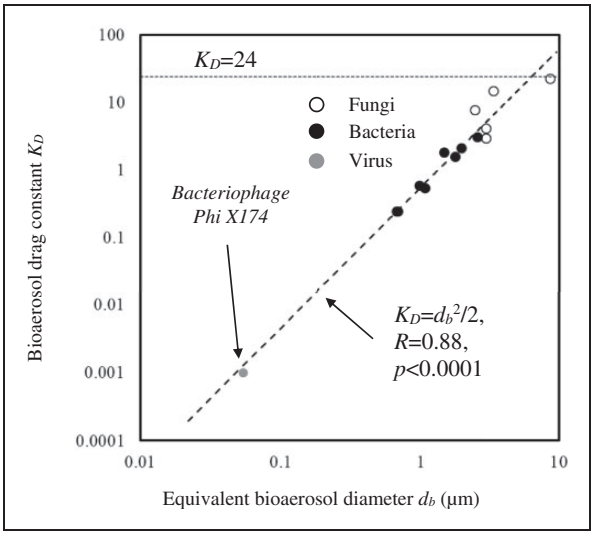

Figure 1. Bioaerosol drag constant K_D against equivalent bioaerosol diameter d_b.

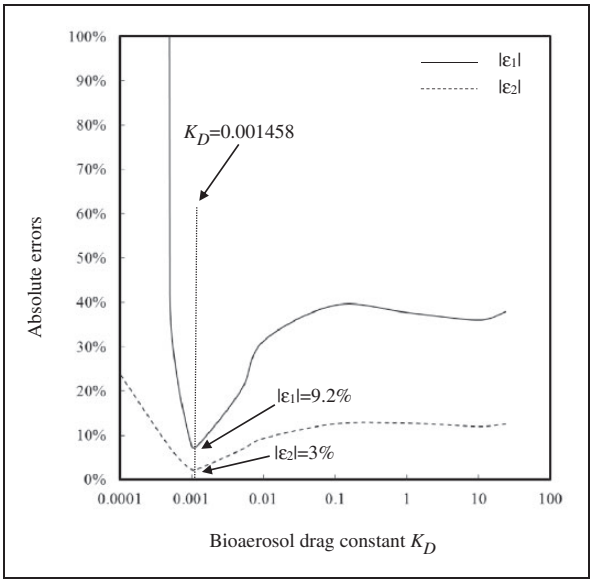

Figure 2. Bioaerosol drag constants and absolute errors for *Bacteriophage Phi X174*.

equation (3) can be extrapolated for predicting the dispersion of smaller sized bioaerosols (down to $d_b = 0.054\,\mu$m). When using $K_D = 0.001458$ (Figure 2), the deviation between simulated and measured fractional counts inside a ventilated chamber was insignificant ($p > 0.99$, paired t-test). The corresponding fractional bias (FB) ε_1 and normalized mean square error (NMSE) ε_2 for $K_D = 0.001458$ were 9.2% and −3%, respectively, as illustrated in Figure 2.[16]

Using equation (4), where the projected image area, length and width are A_b, l_1 and l_2, respectively, the equivalent bioaerosol diameter d_b can be determined from electron micrographs.[17,18] Electron micrographs of samples of MERS-*CoV*, SARS-*CoV*, H1N1 influenza virus and *Bacteriophage Phi X174* are shown in Figure 3.[19–22]

$$d_b = 2\sqrt{\frac{A_b}{\pi}};\ r_{aspect} = \frac{max\,(l_1, l_2)}{min\,(l_1, l_2)} \tag{4}$$

CFD simulation

A typical semi-enclosed six-bed general ward cubicle (7.5 m $(L) \times 6$ m $(W) \times 2.7$ m (H)) employed for the CFD simulation is shown in Figure 4. As illustrated in Figure 5, there were four ceiling air inlets with mounted diffusers in the cubicle, and the corridor was the air-outlet. Four different air change rates (i.e. $ach = 3$, 6, 9 and 13 h^{-1}) were used, while the temperature and relative humidity (RH) of the supply air were 285 K and 80–95%, respectively.[23] Six probable viral emission points, representing the positions of six patients lying on their respective beds (i.e. Man 1, Man 2,. . ., Man 6), were chosen as the source locations. The viruses investigated were MERS-*CoV*, SARS-*CoV* and H1N1 influenza virus. The metabolic rate of a reclining patient was assumed to be 0.8 MET (i.e. 46.6 W m^{-2}).[24] Half of the heat (23.3 W m^{-2}) transferred from patient skin surface by convection was assumed.[25] Patient beds were set as rectangular box

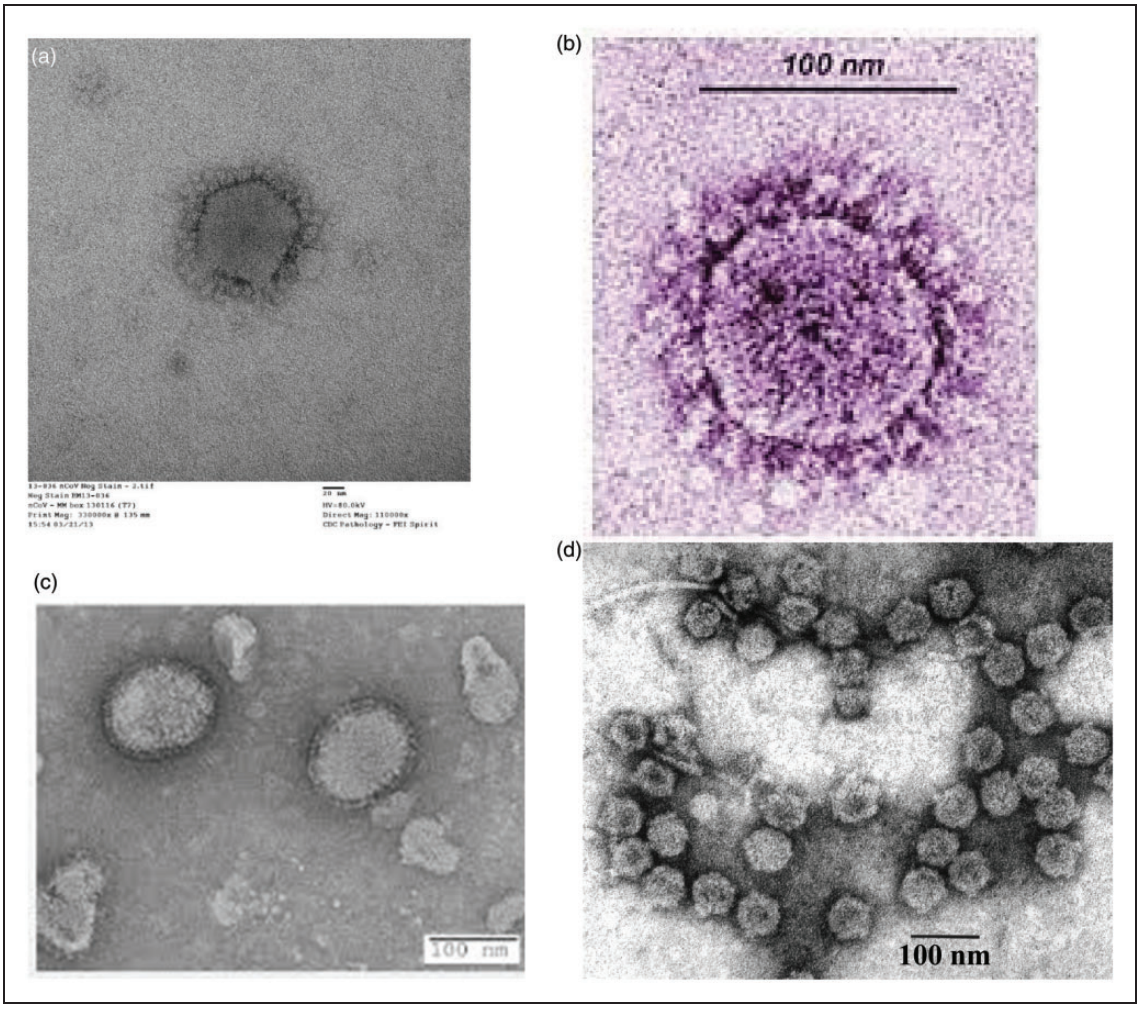

Figure 3. Electron micrograph of reference viruses. (a) MERS-*CoV*[19] (b) SARS-*CoV*[20] (c) H1N1 influenza virus[21] and (d) *Bacteriophage Phi X174*.[22]

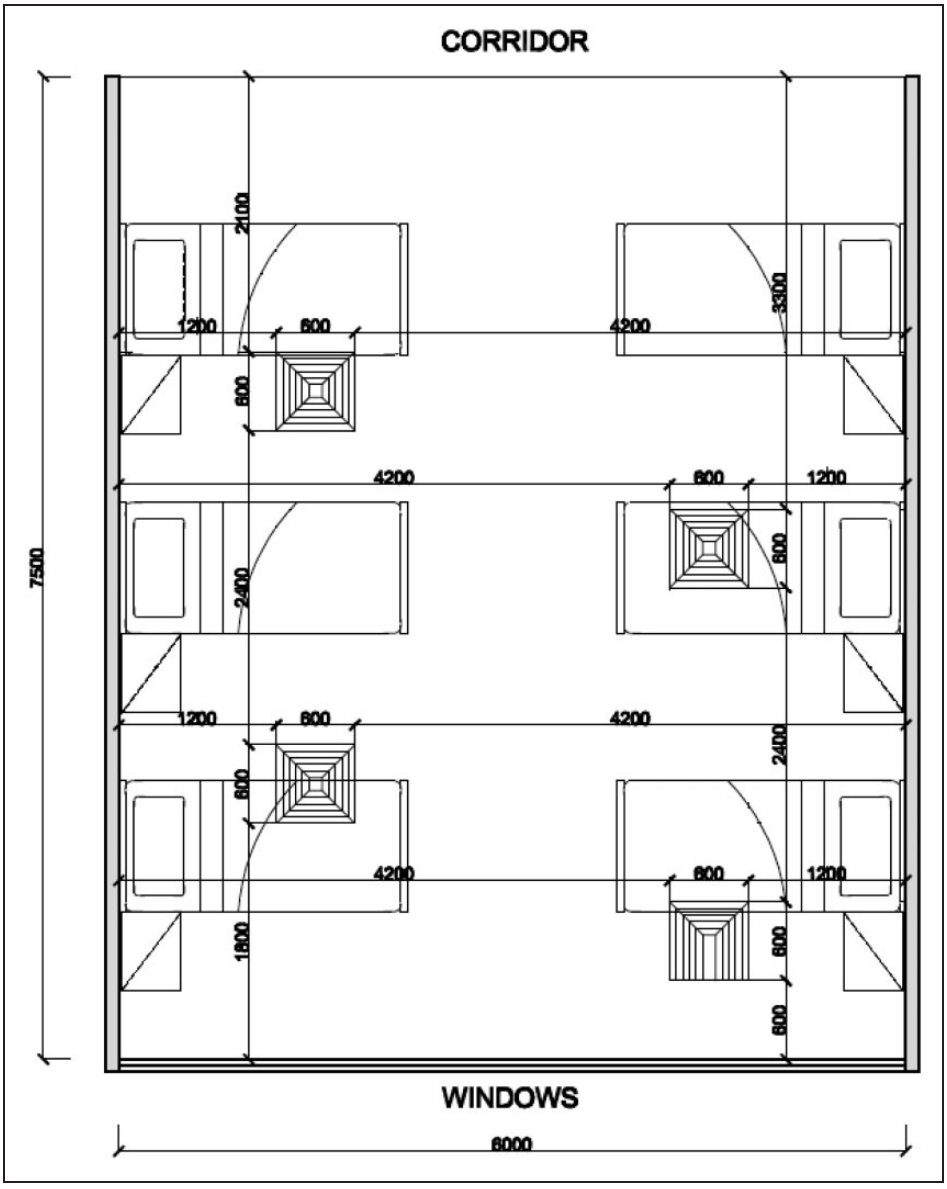

Figure 4. A six-bed general ward cubicle (dimensions in mm).

for the worst scenarios that airflow under the beds was fully blocked by medical equipment and relation installations. This arrangement may cause higher numbers of bioaerosol particle deposited on other patients.

The simulation of airflow field and virus dispersion inside the ward cubicle was done through the use of CFD software FLUENT 14. An Eulerian–Lagrangian framework was used to solve the gas–solid two-phase flow problem, i.e. an Eulerian scheme for the prediction of a steady-state airflow field of the ward cubicle, followed by a Lagrangian approach for the determination of virus particle movements.

In the Eulerian framework, a continuous phase of the induced airflow field was obtained with a second-order solution scheme. The renormalization group (RNG) k-ε turbulence model was tested to be an appropriate choice among the RANS turbulence models, and therefore, it was adopted to determine the air turbulence in the field. The model offered better accuracy and stability in cases of low Reynolds number and near-wall flows, and this model was found suitable for indoor airflow simulations also.[26,27] To couple with the pressure and velocity fields, the pressure implicit with splitting of operator (PISO) algorithm was employed, and the convection term was discretized using a second-order upwind scheme.

To optimize the simulation quality and speed, three reference grid sizes namely fine (i.e. 2618 k), moderate (i.e. 1143 k) and coarse (i.e. 1071 k) were constructed for determining a suitable mesh size. The fine gird

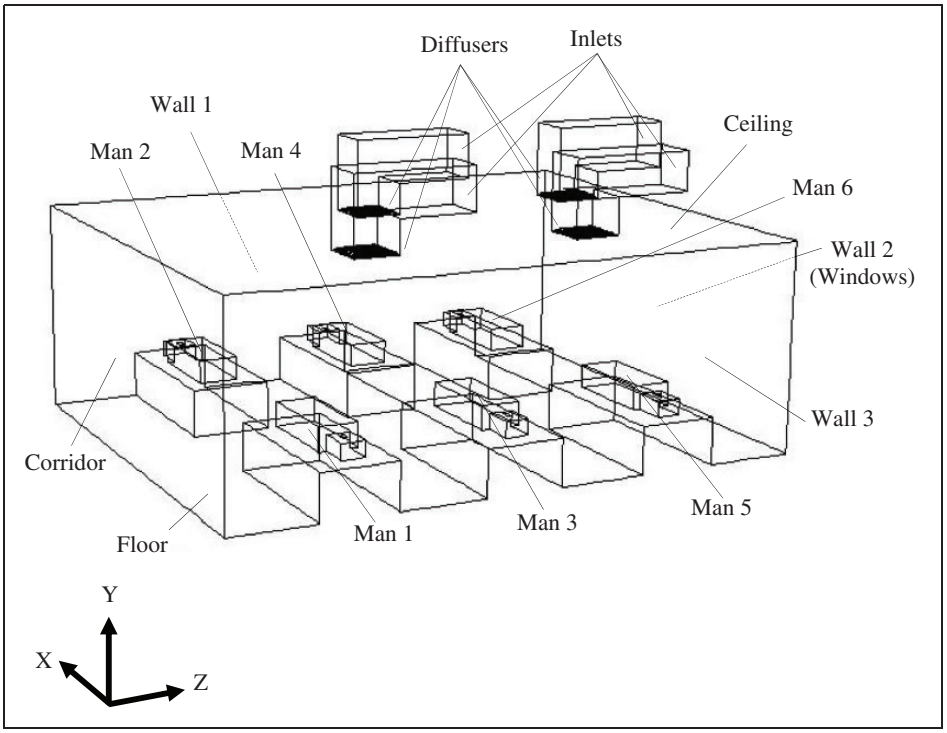

Figure 5. CFD configurations of a six-bed general ward cubicle.

size was with a mesh skewness less than 0.25 to ensure an excellent cell quality. The moderate and coarse grid sizes were doubled and quadrupled by a second-order method for increasing the simulation speed. To assess the mesh quality using linear grid stretching, the asymptotic range of convergence c_{asymp} applied was based on the grid convergence indexes (GCIs) with a relative error of computed average mass flow rate ε_{rms}.[28]

If the value of c_{asymp} in equation (5), where f_s is the safety factor, r_r is the refinement ratio and c_o is the theoretical order of convergence, is approximately 1, then the grid quality is fine.

$$GCI_{fine} = \frac{f_s|\varepsilon_{rms}|}{(r_r^{c_o}-1)};\ GCI_{coarse} = \frac{f_s|\varepsilon_{rms}|r_r^{c_o}}{(r_r^{c_o}-1)};$$
$$c_{asymp} = \frac{GCI_{coarse}}{(GCI_{fine})r_r^{c_o}} \quad (5)$$

The GCI analysis results from the simulation were 51%, 37% and 1.187 for GCI_{coarse}, GCI_{fine} and c_{asymp}, respectively.

In the CFD simulation, the transmission pathway of virus-laden respiratory droplets expelled by sneezing was predicted (i.e. d_i, initial virus-laden respiratory droplets diameter = 8.3 μm, $v_b = 50\,\mathrm{m\ s^{-1}}$, $\rho_b = 1100\,\mathrm{kg\ m^{-3}}$ and n_s, amount of virus particles expelled by sneezing = 10,000 virus particles).[14,29–31] General patient wards are recommended at an RH 30–60%.[6] Within a short period of time (<0.1 s) after emission, the droplets would evaporate to droplet nuclei.[32] These nuclei were the dried-out residual of droplets possibly containing infectious pathogens.[33] Only a small proportion (<10%) of the virus-laden droplets of a total number of 73,000–1,000,000 droplets expelled by a vigorous sneeze was assumed; neither aggregation with other particles nor cluster of virus would be formed from the dried-out nuclei at such low concentration.[34,35] Lipid-enveloped human coronavirus 299 E would remain alive by a half-life of 67 h at an RH of 50% and an air temperature of 20°C.[36] The survival rate of the three virus was expected to be 100% in simulation times less than 100 s. Other details for simulations and boundary conditions are summarized in Table 1.

Table 2 exhibits the equivalent bioaerosol diameters d_b for the virus droplet nuclei examined in this study. A one-way coupling was applied in the prediction to prevent the effect of particles on the continuum airflow. Each virus particle was tracked separately for its position and velocity by a discrete phase model (DPM). A previous study confirmed that the isotropic discrete random walk (DRW) model was effective and accurate in modelling bioaerosol dispersion and distribution due to turbulent fluctuations in the flow.[37] For a coagulation effect of bioaerosol particles in this study, a very low volume fraction ($<3000\,\mathrm{cm^{-3}}$) was kept in the ward cubicle to reduce collisions of the virus particles in

a turbulent flow.[38,39] Both the amounts of virus particles exhausted to the corridor n_e and deposited on the ward room surfaces n_d were counted.[40] A perfect sink boundary condition was applied to the ward room surfaces in order that the virus particles impinged onto the solid surfaces would be perfectly trapped with no reflection and desorption.[41]

Table 1. CFD simulations and boundary conditions.

Computational domain	7.5 m (L) × 6 m (W) × 2.7 m (H), RNG k-ε turbulence model, standard wall function.
Mesh configuration	1,143,766 cells
Total supply airflow rate	1.24 kg s^{-1} (for $ach = 3$), 2.48 kg s^{-1} (for $ach = 6$), 3.72 kg s^{-1} (for $ach = 9$) and 5.37 kg s^{-1} (for $ach = 13$), 285 K (air temperature)
Each inlet airflow rate (0.6 m × 0.6 m)	0.31 kg s^{-1} (for $ach = 3$), 0.62 kg s^{-1} (for $ach = 6$), 0.93 kg s^{-1} (for $ach = 9$) and 1.34 kg s^{-1} (for $ach = 13$), 285 K (air temperature)
Four diffuser (0.6 m × 0.6 m)	Four-way spread-type, supply jets had an angle of 15° from ceiling, adiabatic and reflect boundary type.
Corridor (6 m × 2.7 m)	Pressure-outlet, 295 K (backflow temperature), adiabatic, escape boundary type.
Walls, ceiling, floor and beds	No slip wall boundary, 295 K (surface temperature), adiabatic, trap boundary type.
Patients	No slip wall boundary, 23.3 W m^{-2}, trap boundary.
Patient mouths (0.05 m × 0.05 m)	Single-shot release with an upward exhalation velocity of $v_b = 50$ m s^{-1}, initial virus-laden respiratory droplet diameter $d_i = 8.3$ μm, $n_s = 10{,}000$ virus particles, density of bioaerosol particle $\rho_b = 1100$ kg m^{-3}

RNG: renormalization group.

Deposited ratio

Direct contact with the viruses deposited on ward room surfaces and inhalation of the viruses suspended in the air are two potential transmission routes of virus-laden airborne particles expelled by sneezing.[42] The deposited ratio r_d is selected as a measure for evaluating the contact transmission; the movement of sneeze particles can be represented by equation (6), where r_e is the exhausted ratio for particles exhausted to the corridor and r_a is the elapsed ratio for particles suspended in the air

$$r_e + r_a + r_d = 1 \tag{6}$$

Ratios r_e, r_a and r_d are given by equation (7), where n_s, n_e, n_a and n_d are the amounts of virus particles expelled by sneezing, exhausted to the corridor, elapsed

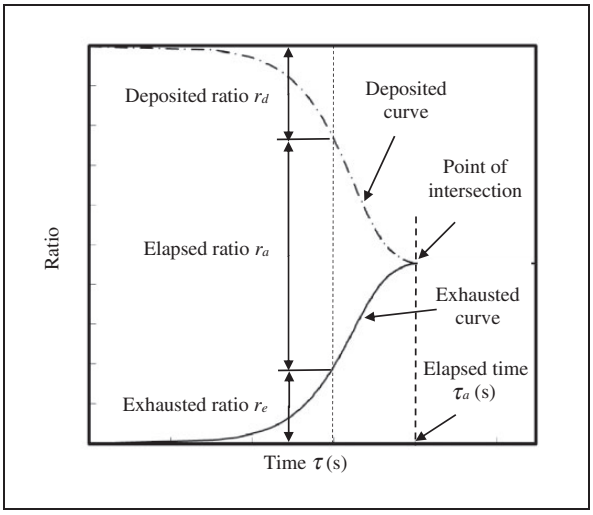

Figure 6. Description of the bioaerosol removal process in a general ward.

Table 2. Virus information.

Species	ATCC	Equivalent bioaerosol diameter d_b (μm)[a]	Aspect ratio (r_{aspect})	Drag constant K_D	Evaporation time at 0% RH (s)	Evaporation time at 50% RH (s)	Evaporation time at 90% RH (s)
MERS-*CoV*	–	0.167 ± 0.012	1.27	0.013945	3.48×10^{-2}	9.55×10^{-2}	1.82×10^{-1}
SARS-*CoV*	–	0.1375 ± 0.009	1.052	0.009453	3.48×10^{-2}	9.55×10^{-2}	1.82×10^{-1}
H1N1 influenza virus	–	0.124 ± 0.0001	1.203	0.0199	3.48×10^{-2}	9.55×10^{-2}	1.82×10^{-1}
Bacteriophage Phi X174	13706-B1	0.054 ± 0.014	1.012	0.001458	–	–	–

MERS-*CoV*: Middle East respiratory syndrome coronavirus; SARS-*CoV*: severe acute respiratory syndrome coronavirus.
[a]Standard errors shown.

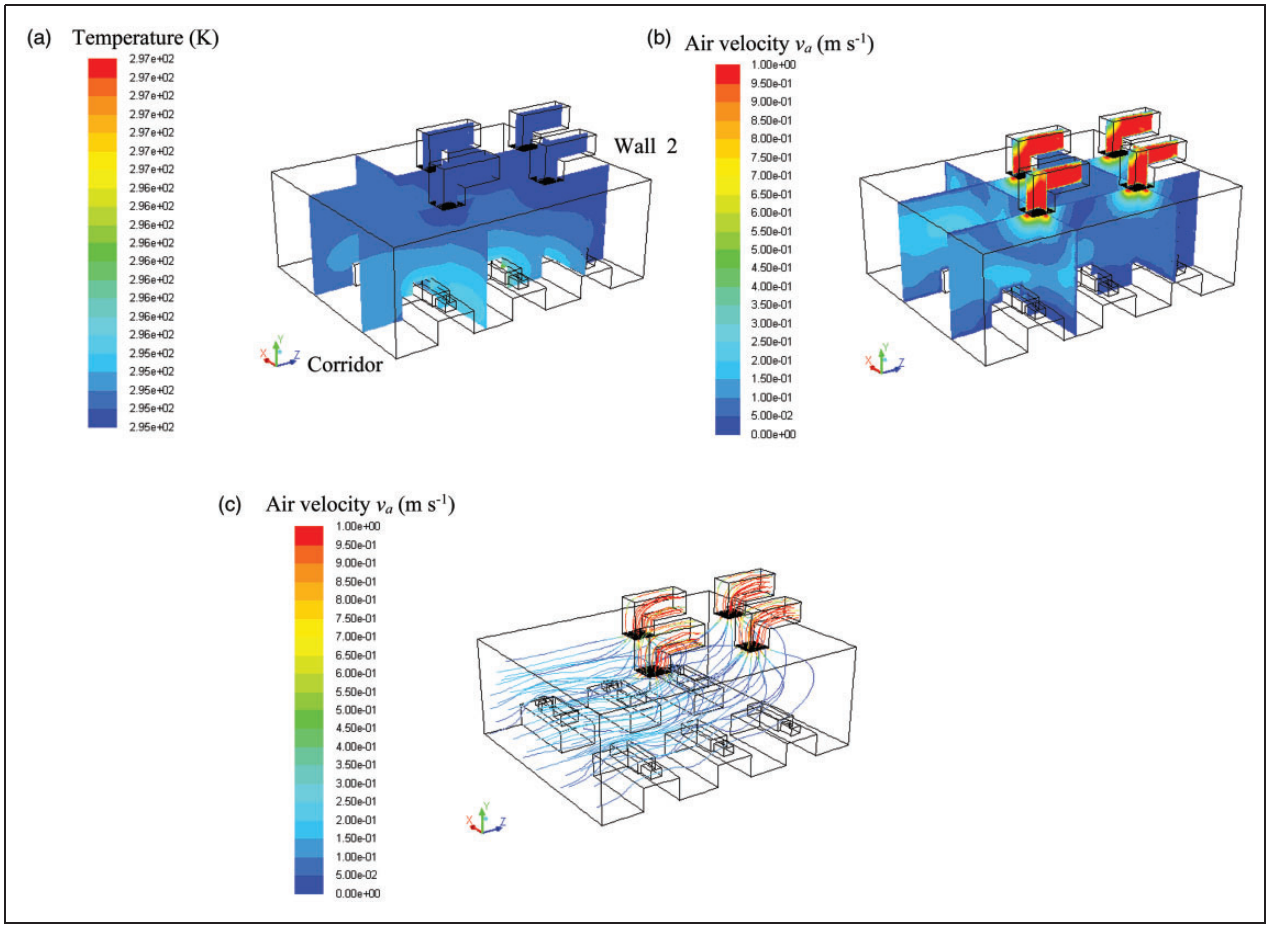

Figure 7. Simulation results of the ward with $ach = 6\,h^{-1}$. (a) Temperature distribution, (b) air velocity distribution and (c) flow pathlines from air supply inlets.

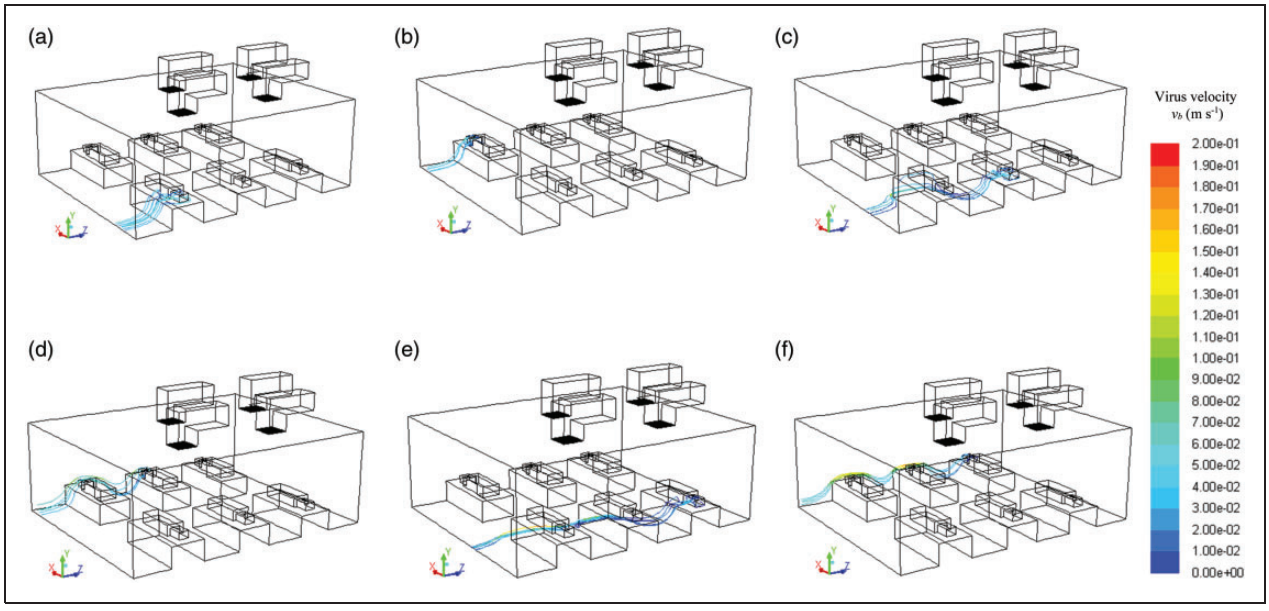

Figure 8. MERS-*CoV* pathways for six source locations with $ach = 6\,h^{-1}$. (a) Man 1, (b) Man 2, (c) Man 3, (d) Man 4, (e) Man 5 and (f) Man 6.

(with respect to air suspension) and deposited on ward room surfaces, respectively

$$r_e = \frac{n_e}{n_s};\ r_a = \frac{n_a}{n_s};\ r_d = \frac{n_d}{n_s} \tag{7}$$

Figure 6 graphs the ratios r_e, r_a and r_d against time. The elapsed time τ_a (s) required for all virus particles to be exhausted or to deposit on ward room surfaces can be determined from the figure as represented by equation (8).

$$r_a(\tau_a) = 0 \tag{8}$$

Results and discussion

Airflow field

Figure 7 shows the simulated temperature, air velocity distribution and the flow pathlines inside the ward with $ach = 6\,h^{-1}$. An increasing temperature gradient was found from the ceiling to the floor inside the ward. As shown in Figure 7(a), warmer air observed near the patients (due to body temperature) was diffusing out to the corridor. The average room temperature was about 296 K. Stagnant air, with velocity less than 0.05 m s^{-1}, was found near the window side (i.e. Wall 2) and the

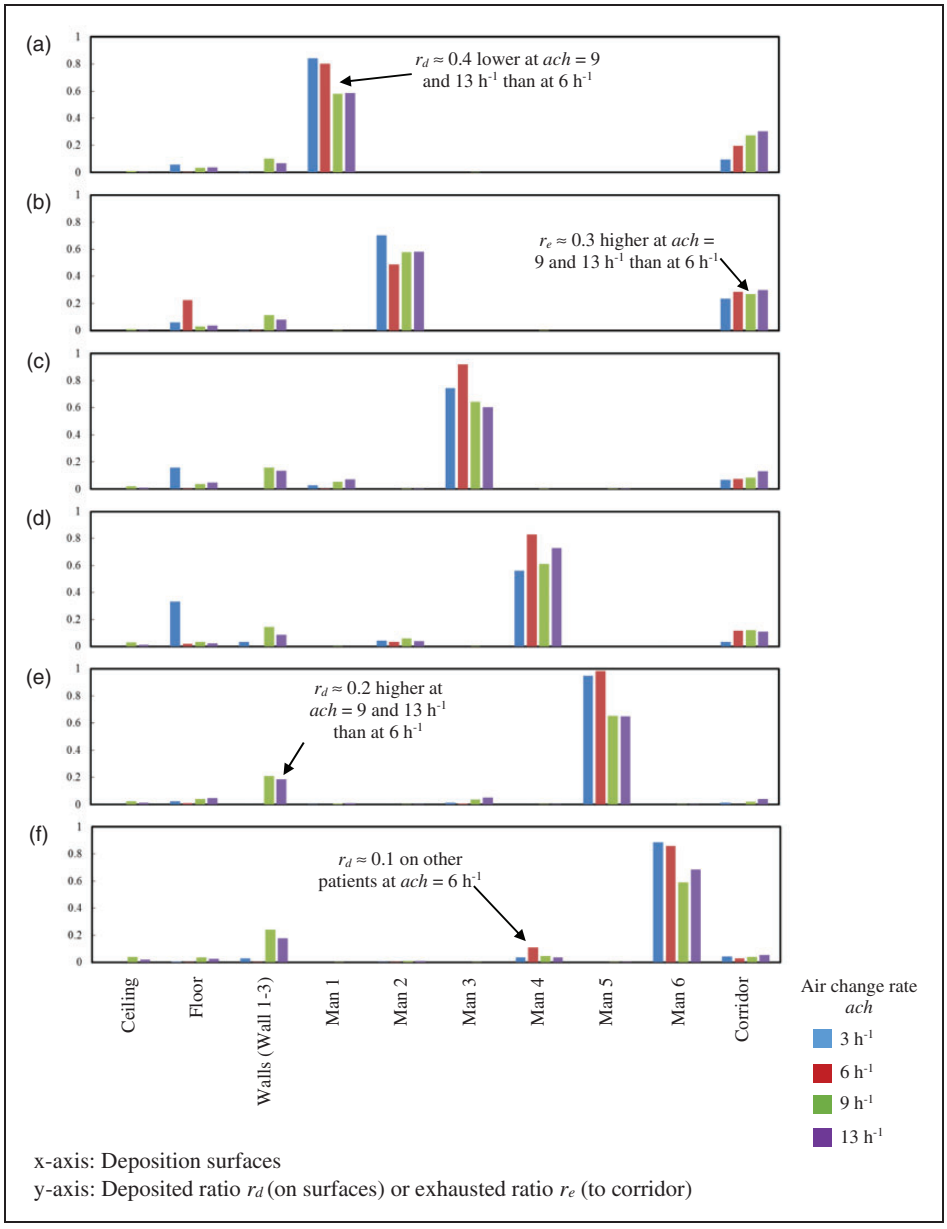

Figure 9. Deposited and exhausted ratios of MERS-*CoV* for six source locations. (a) Man 1, (b) Man 2, (c) Man 3, (d) Man 4, (e) Man 5 and (f) Man 6.

lower floor level (i.e. below 0.3 m) as presented in Figure 7(b). The flow pathlines in Figure 7(c) confirm that there was insufficient ventilation to remove any virus particles in those areas. Generally, the airflow direction was from the inner part of the ward to the corridor.

Cross-infection from surface deposition

Figure 8 indicates the potential risks of cross-infection with MERS-*CoV* through air pathways from different infected patients inside the ward. Patients staying on the same side of an infected patient, especially the one located next to the corridor (i.e. Man 1 or Man 2), would have a higher chance of cross-infection. Two different virus pathway flows in the simulation due to the asymmetric diffuser locations are highlighted. Cases exhibited in Figure 8(c) and (e) show the virus moved along floor surface of the ward but in cases shown in Figure 8(d) and (f), virus would pass over nearby patients' heads, then flew to the corridor.

Figure 9 exhibits the values of deposited ratio r_d and exhausted ratio r_e of MERS-*CoV* on all surfaces inside the ward with $ach = 3$, 6, 9 and 13 h^{-1}. The results suggested that the deposition of virus particles was dependent on the location of an infected patient, and the virus particles would deposit mainly back on the source patient. If the infected patient was located near the corridor (i.e. Man 1 or Man 2), the virus particles would likely be exhausted to the corridor. On the contrary, if the infected patient was located in the inner part of the ward (i.e. Man 5 or Man 6), the possibility that the virus particles would deposit on the wall surfaces or other patients was higher.

Moreover, more virus particles would remain on the sneezing patient at lower air change rates, especially for $ach = 6\,h^{-1}$ ($r_d > 0.7$ for all source locations), whereas more virus particles would deposit on the wall surfaces or be exhausted to the corridor at higher air change rates (i.e. $ach = 9\,h^{-1}$ or $13\,h^{-1}$). Although the possibility of cross-infection among patients and healthcare workers (HCWs) was lower at a higher *ach* (up to $9\,h^{-1}$), HCWs should clean all patients and ward surfaces regularly, regardless of *ach*.

Cross-infection from inhalation

Figure 10 graphs the MERS-*CoV* removal processes in the ward for the six source locations (i.e. Man 1, Man 2,. . ., Man 6) and $ach = 3$, 6, 9 and 13 h^{-1}. The results showed that virus particles from an infected patient located near the corridor were likely to be exhausted to the corridor. Meanwhile, lower r_e (i.e. higher r_d) and longer elapsed time τ_a were associated with the MERS-*CoV* particles from the sneezing of an infected patient located in the inner part of the ward, and that indicated a higher risk of MERS-*CoV* infection through direct inhalation of particles or indirect inhalation of re-suspended particles. Besides, higher r_e and shorter τ_a were found with increasing air change rates. If *ach* was increased from 3 to 13 h^{-1}, τ_a could be shortened by more than 30 s, and the risk of cross-infection from inhalation could be effectively lowered. Similar dispersion and deposition results were observed for SARS-*CoV* and H1N1 influenza virus particles and pictorialized in Figures 11 and 12. The simulation performances demonstrated that virus particles with a relatively small equivalent bioaerosol diameter ($d_b \sim 0.1\,\mu$m) had similar particle dispersion and deposition characteristics in a general hospital ward.

Figure 13 plots the average elapsed time τ_a against *ach* for MERS-*CoV*, SARS-*CoV* and H1N1 influenza virus. The results showed that τ_a could be significantly shortened by increasing the air change rate in the ward ($R^2 > 0.9$). However, the threshold or optimal τ_a in the ward could not be determined as the infectious doses (ID50) of the three viruses varied in wide ranges (i.e. 180, 1800 and 180 virus particles for MERS-*CoV*, SARS-*CoV* and H1N1 influenza virus, respectively, to cause a 50% infection).[43–45] Using the ASHRAE standard for an AIIR (i.e. $ach = 12\,h^{-1}$) as a safety measure,[6] the corresponding elapsed time was about 34 s. When applying the ASHRAE ($ach = 4\,h^{-1}$) and CIBSE ($ach = 6\,h^{-1}$) standards for a general patient room, the average values of τ_a were found to be 70 s and 61 s, respectively.[6,8] The elapsed time doubled when *ach* dropped from 12 to $4\,h^{-1}$, and thus doubling the potential inhalation risk. Based on the median value in accordance with both ASHRAE and CIBSE standards, the maximum *ach* in a general hospital ward should be $9\,h^{-1}$ ($\tau_a = 48$ s) for the needs of maximizing energy efficiency and minimizing infection risk. Furthermore, it should be noted for other means to minimize the possibility of cross-contamination in hospital wards, such as the installation of ultraviolet germicidal irradiation (UVGI) lamps for the destruction of viral nucleic acids.[46]

Conclusion

This study should provide a useful source of reference for the hospital management to mitigate the risk of infection with MERS or other airborne transmitted viruses through better ventilation design strategies. The results of this study demonstrated that the location of an infected patient would affect the infection risks to other occupants and HCWs inside the same hospital ward, and an increased air change rate in the ward could reduce the risk of infection from direct contact

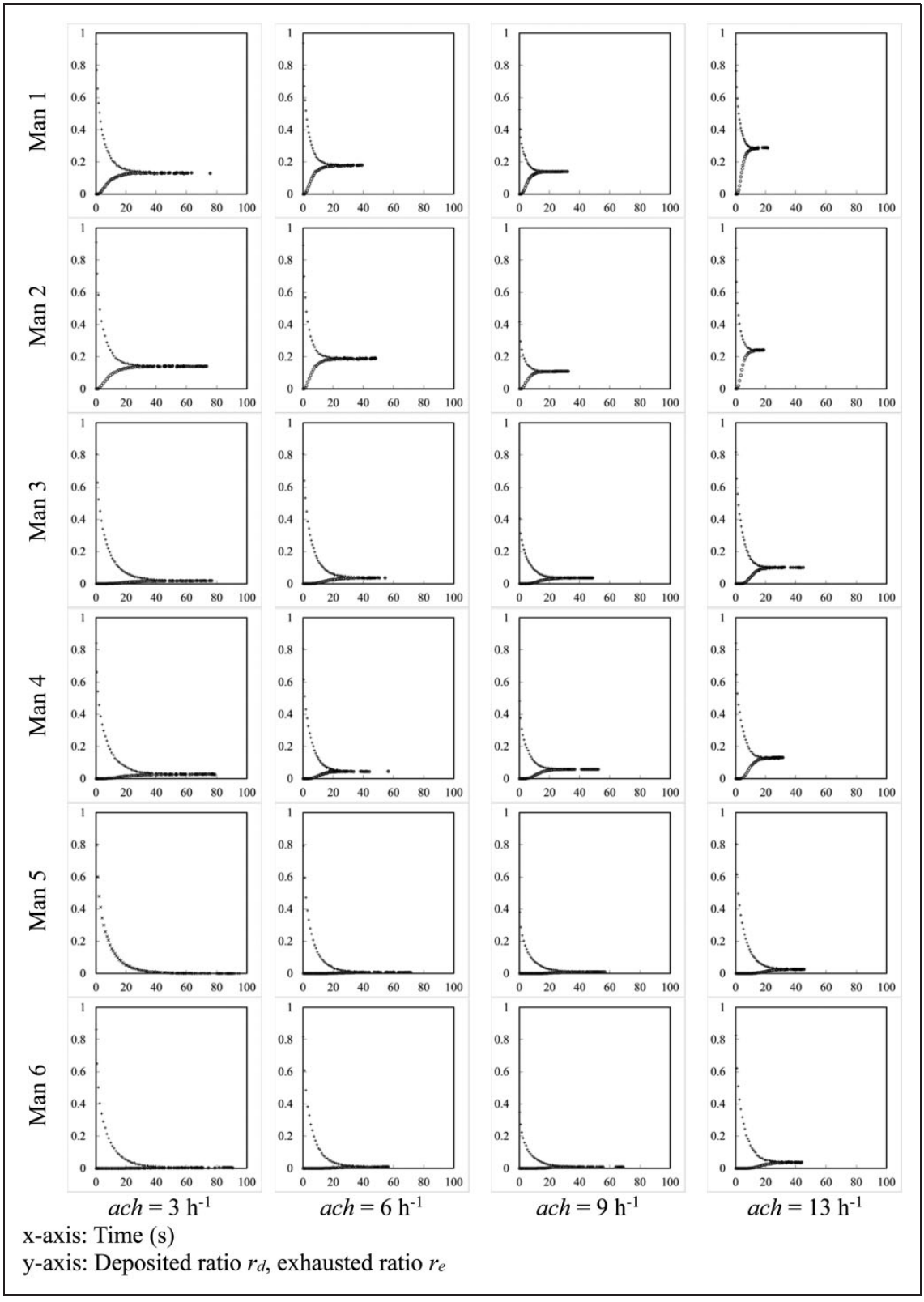

Figure 10. MERS-*CoV* removal processes for different source locations and air change rates.

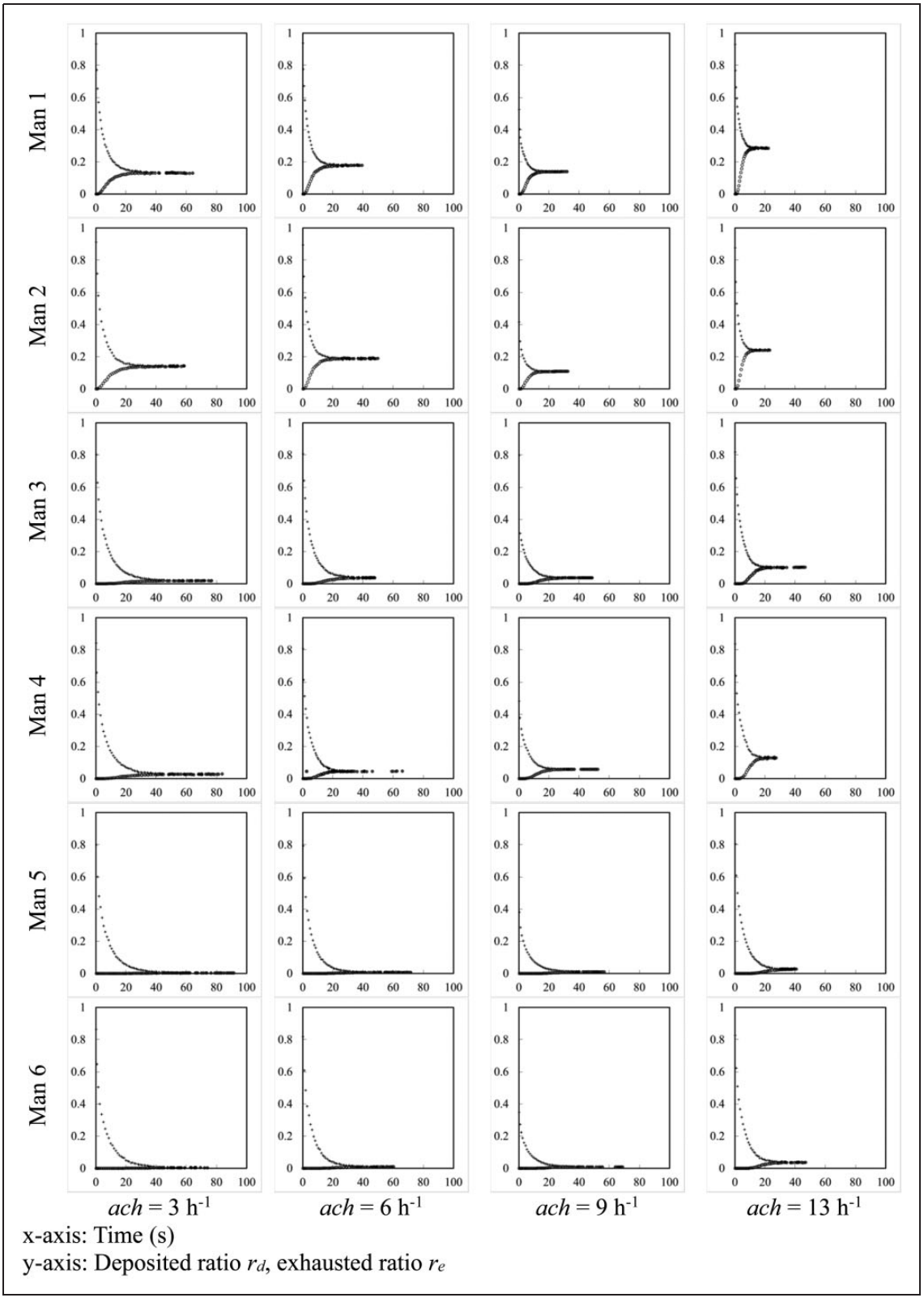

Figure 11. SARS-*CoV* removal processes for different source locations and air change rates.

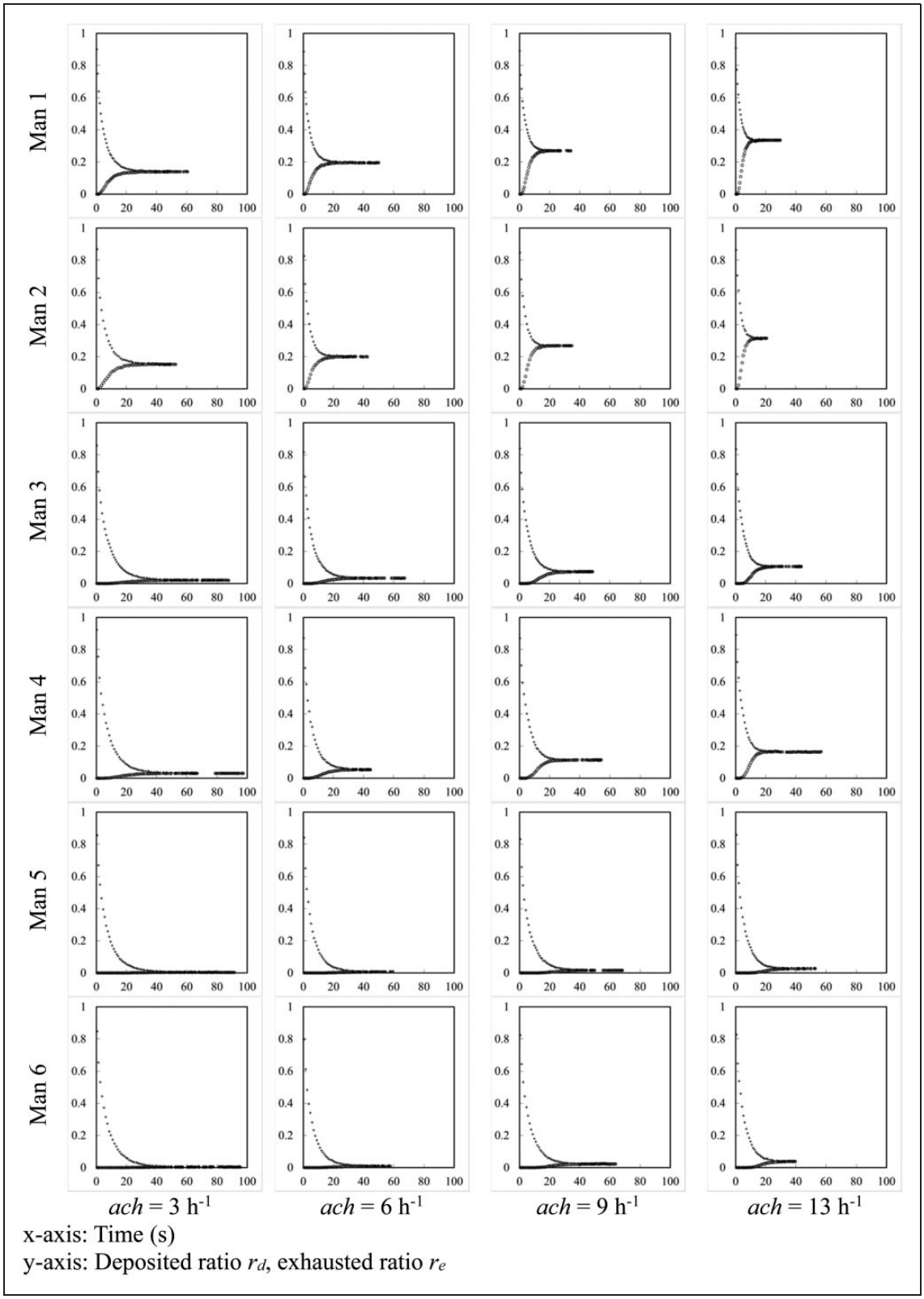

Figure 12. H1N1 influenza virus removal processes for different source locations and air change rates.

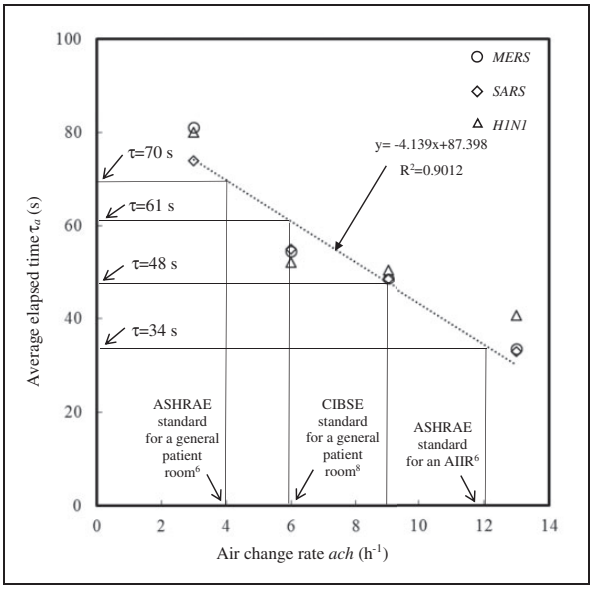

Figure 13. Average elapsed time τ_a with design standards. MERS: Middle East respiratory syndrome; SARS: severe acute respiratory syndrome; AIIR: airborne infection isolation room.

and inhalation. For a typical semi-enclosed six-bed general ward of Hong Kong hospitals, an air change rate of $9\,h^{-1}$ could effectively minimize the deposition and floating time of respiratory virus particles while maximizing energy efficiency. In order to minimize the possibility of cross-contamination in hospital wards, installation of UVGI lamps is also recommended.

Author's contribution

All authors contributed equally in the preparation of this manuscript.

Declaration of conflicting interests

The author(s) declared no potential conflicts of interest with respect to the research, authorship, and/or publication of this article.

Funding

The author(s) disclosed receipt of the following financial support for the research, authorship, and/or publication of this article: This research project was funded by the Public Policy Research Funding Scheme from the Central Policy Unit of the Hong Kong Special Administrative Region Government (Project Number: 2014.A6.038.14E) and The Hong Kong Polytechnic University (Project Numbers G-YBA7 and G-YK22).

References

1. HKMA. *Hosptial authority statistical report 2012-2013*. Hong Kong: Hong Kong Hospital Authority, 2014.
2. CDC. *Guideline for isolation precautions: preventing transmission of infectious agents in healthcare settings*. Altanta, GA: Centers for Disease Control and Prevention, 2007.
3. Kupferschmidt K. Did poor ventilation lead to MERS 'superspread' in Korea? *ScienceInsider,* http://news.sciencemag.org/asiapacific/2015/06/did-poor-ventilation-lead-mers-superspread-korea-triggers-mers-explosion-south-korea (2015, accessed 5 June 2015). DOI: 10/1126/science.aac4673.
4. Tomlinson B and Cockram C. SARS: experience at Prince of Wales Hospital, Hong Kong. *Lancet* 2003; 361: 1486–1487.
5. Li Y, Huang X, Yu ITS, Wong TW and Qian H. Role of air distribution in SARS transmission during the largest nosocomial outbreak in Hong Kong. *Indoor Air* 2005; 15: 83–95.
6. ASHRAE Standard 170 – 2013. *Ventilation for health care facilities*. Atlanta, GA: American Society of Heating, Refrigerating and Air-Conditioning Engineers, Inc., 2013.
7. Yau YH, Chandrasegaran D and Badarudin A. The ventilation of multiple-bed hospital wards in the tropics: a review. *Build Environ* 2011; 46: 1125–1132.
8. CIBSE. Guide B2. *Heating, ventilating, air conditioning and refrigeration*. London: Chartered Instituation of Building Services Engineers, 2005.
9. Short CA and Al-Maiyah S. Design strategy for low-energy ventilation and cooling of hospitals. *Build Res Inf* 2009; 37: 264–292.
10. Shepley MM and Song Y. Design research and the globalization of healthcare environments. *HERD J* 2014; 8: 158–198.
11. Ninomura P and Bartley J. New ventilation guidelines for healthcare facilities. *ASHRAE J* 2001; 43: 29–33.
12. ASHRAE Standard 62.1-2013. *Ventilation for acceptable indoor air quality*. Atlanta, GA: American Society of Heating, Refrigerating and Air-Conditioning Engineers, Inc., 2013.
13. Darwich A. ASHRAE Standard 170 Update. *AHSRAE 2014 NYC Winter and Seattle Summer Meetings*. Sacramento, CA: Guttmann and Blaevoet Consulting Engineers, 2014.
14. Wong LT, Yu HC, Mui KW and Chan WY. Drag constants of common indoor bioaerosols. *Indoor Built Environ* 2015; 24: 401–413.
15. Sze To GN, Wan MP, Wei F, Chao CYH, Yu SCT and Kwan JKC. Estimation of exposure levels of virus – laden expiratory aerosals in a hospital ward under imperfect mixing condition. In: *IAQVEC 2007 proceedings – 6th international conference on indoor air quality, ventilation and energy conservation in buildings: sustainable built environment*. Sendai, Japan: Tohoku University press, 2007, pp.321–328.
16. ASTM D6589-05(2010)e1. *Standard guide for statistical evaluation of atmospheric dispersion model performance*. West Conshohocken, PA: American Society for Testing and Materials, 2010.
17. Ferreira T and Rasband W. *ImageJ User Guide/Fiji 1.46*. Bethesda, MD: U.S. National Institutes of Health, 2012.
18. Wagner J and Macher J. Automated spore measurements using microscopy, image analysis, and peak recognition of near-monodisperse aerosols. *Aerosol Sci Tech* 2012; 46: 862–873.
19. Goldsmith CS and Tamin A. *MERS-CoV photos*. Centers for Disease Control and Prevention, http://www.cdc.gov/coronavirus/mers/photos.html (2015, accessed 28 June 2015).
20. Ksiazek TG, Erdman D, Goldsmith CS, Zaki SR, Peret T, Emery S, Tong S, Urbani C, Comer JA, Lim W, Rollin PE, Dowell SF, Ling AE, Humphrey CD, Shieh WJ, Guarner J, Paddock CD, Rota P, Fields B, DeRisi J, Yang JY, Cox N, Hughes JM, LeDuc JW, Bellini WJ, Anderson LJ, and the SARS and working Group. A novel coronavirus associated with severe acute respiratory syndrome. *New Engl J Med* 2003; 348: 1953–1966.
21. Bio Materials Analysis Technology Inc., http://www.biomatek.com/Services_B1-1-3.html (2014, accessed 28 June 2015).

22. Ackermann H. Coliphage phiX174. ICTVdB picture gallery, http://ictvdb.bio-mirror.cn/Images/Ackerman/Phages/Microvir/238-27.htm (2002, accessed 28 June 2015).
23. Qian H, Li Y, Nielsen PV, Hyldgaard CE, Wong TW and Chwang ATY. Dispersion of exhaled droplet nuclei in a two-bed hospital ward with three different ventilation systems. *Indoor Air* 2006; 16: 111–128.
24. ASHRAE. *ASHRAE Fundamentals SI Handbook*. Atlanta, GA: American Society of Heating, Refrigerating and Air-Conditioning Engineers, Inc., 2013.
25. Hang J, Li Y and Jin R. The influence of human walking on the flow and airborne transmission in a six-bed isolation room: tracer gas simulation. *Build Environ* 2014; 77: 119–134.
26. Zhang Z, Zhang W, Zhai Z and Chen Q. Evaluation of various turbulence models in predicting airflow and turbulence in enclosed environments by CFD: Part-2: comparison with experimental data from literature. *HVAC&R Res* 2007; 13: 871–876.
27. Launder BE and Sharma BI. Application of the energy-dissipation model of turbulence to the calculation of flow near a spinning disc. *Lett Heat Mass Trans* 1974; 1: 131–137.
28. Roache PJ. Verification of codes and calculations. *AIAA J* 1998; 36: 696–702.
29. Yang S, Lee GWM, Chen C-M, Wu C-C and Yu K-P. The size and concentration of droplets generated by coughing in human subjects. *J Aerosol Med* 2007; 20: 484–494.
30. Mui KW, Wong LT, Wu CL and Lai ACK. Numerical modeling of exhaled droplet nuclei dispersion and mixing in indoor environments. *J Hazard Mater* 2009; 167: 736–744.
31. Gupta JK, Lin CH and Chen Q. Flow dynamics and characterization of a cough. *Indoor Air* 2009; 19: 517–525.
32. Xie X, Li Y, Chwang ATY, Ho PL and Seto WH. How far droplets can move in indoor environments – revisiting the wells evaporation–falling curve. *Indoor Air* 2007; 17: 211–225.
33. Wells WF. *Airborne contagion and air hygiene*. Cambridge, MA: Cambridge University Press, 1955.
34. Duguid JP. The size and the duration of air-carriage of respiratory droplets and droplet-nuclie. *J Hyg* 1946; 44: 471–479.
35. Gralton J, Tovey E, McLaws ML and Rawlinson WD. The role of particle size in aerosolised pathogen transmission: a review. *J Infect* 2011; 62: 1–13.
36. Tang JW, Li Y, Eames I, Chan PKS and Ridgway GL. Factors involved in the aerosol transmission of infection and control of ventilation in healthcare premises. *J Hops Infect* 2006; 64: 100–114.
37. Lai ACK, Wong LT, Mui KW, Chan WY and Yu HC. An experimental study of bioaerosol (1-10um) deposition in a ventilated chamber. *Build Environ* 2012; 56: 118–126.
38. Hussein T, Hruška A, Dohányosová P, Džumbová L, Hemerka J, Kulmala M and Smolik J. Deposition rates on smooth surfaces and coagulation of aerosol particles inside a test chamber. *Atmos Environ* 2009; 43: 905–914.
39. Rim D, Green M, Wallace L, Persily A and Choi JI. Evolution of ultrafine particle size distributions following indoor episodic releases: relative importance of coagulation, deposition and ventilation. *Aerosol Sci Tech* 2012; 46: 494–503.
40. Zhao B, Zhan Y, Li X, Yang X and Huang D. Comparison of indoor aerosol particle concentration and deposition in different ventilated rooms by numerical method. *Build Environ* 2004; 39: 1–8.
41. Qian H and Li Y. Removal of exhaled particles by ventilation and deposition in a multibed airborne infection isolation room. *Indoor Air* 2010; 20: 284–297.
42. Sze To GN, Yang Y, Kwan JKC, Yu SCT and Chao CYH. Effects of surface matherial, ventilation, and human behavior on indiret contact transmission risk of respiratory infection. *Risk Anal* 2014; 34: 818–830.
43. de Wilde AH, Raj VS, Oudshoorn D, Bestebroer TM, van Nieuwkoop S, Limpens RW, Posthuma CC, van der Meer Y, Bárcena M, Haagmans BL, Snijder EJ and van den Hoogen BG. MERS-coronavirus replication induces severe in vitro cytopathology and is strongly inhibited by cyclosporin A or interferon-alpha treatment. *J Gen Virol* 2013; 94: 1749–1760.
44. Sze To GN, Wan MP, Chao CY, Wei F, Yu SC and Kwan JK. A methodology for estimating airborne virus exposures in indoor environments using the spatial distribution of expiratory aerosols and virus viability characteristics. *Indoor Air* 2008; 18: 425–438.
45. Koster F, Gouveia K, Zhou Y, Lowery K, Russell R, MacInnes H, Pollock Z, Layton RC, Cromwell J, Toleno D, Pyle J, Zubelewicz M, Harrod K, Sampath R, Hofstadler S, Gao P, Liu Y and Cheng YS. Exhaled aerosol transmission of pandemic and seasonal H1N1 influenza viruses in the ferret. *PLoS ONE* 2012; 7: e33118.
46. Kanaan M, Ghaddar N, Ghali K and Araj G. New airborne pathogen transport model for upper-room UVGI spaces conditioned by chilled ceiling and mixed displacement ventilation: enhancing air quality and energy performance. *Energy Convers Manag* 2014; 85: 50–61.